Draft version April 19, 2017
Preprint typeset using LaTeX style AASTeX6 v. 1.0

arXiv:1702.06541v2 [astro-ph.GA] 18 Apr 2017

REVISITING THE TALE OF HERCULES: HOW STARS ORBITING THE LAGRANGE POINTS VISIT THE SUN

Angeles Pérez-Villegas[1], Matthieu Portail, Christopher Wegg and Ortwin Gerhard
Max-Planck-Institut für Extraterrestrische Physik, Gießenbachstraße, D-85741 Garching, Germany
(Received; Revised; Accepted)

[1]mperez@mpe.mpg.de

Abstract

We propose a novel explanation for the Hercules stream consistent with recent measurements of the extent and pattern speed of the Galactic bar. We have adapted a made-to-measure dynamical model tailored for the Milky Way to investigate the kinematics of the solar neighborhood (SNd). The model matches the 3D density of the red clump giant stars (RCGs) in the bulge and bar as well as stellar kinematics in the inner Galaxy, with a pattern speed of $39\,\mathrm{km\,s^{-1}\,kpc^{-1}}$. Cross-matching this model with the *Gaia* DR1 TGAS data combined with RAVE and LAMOST radial velocities, we find that the model naturally predicts a bimodality in the U–V-velocity distribution for nearby stars which is in good agreement with the Hercules stream. In the model, the Hercules stream is made of stars orbiting the Lagrange points of the bar which move outward from the bar's corotation radius to visit the SNd. While the model is not yet a quantitative fit of the velocity distribution, the new picture naturally predicts that the Hercules stream is more prominent inward from the Sun and nearly absent only a few 100 pc outward of the Sun, and plausibly explains that Hercules is prominent in old and metal-rich stars.

Keywords: Galaxy: kinematics and dynamics — Galaxy: structure — solar neighborhood

1. INTRODUCTION

Hipparcos data clearly revealed the rich substructure in the velocity distribution of solar neighborhood (SNd) stars (Dehnen 1998). Previously, Eggen (1996) had related this structure with moving groups of stars that retain the kinematic signature of their birth places. However, the kinematically identified groups also contain old and late-type stars (Dehnen 1998; Antoja et al. 2008), and some may be related to orbit structures caused by the Galactic bar or spiral arms (Dehnen 2000; Quillen & Minchev 2005).

One of the most studied kinematic group is known as the Hercules stream (or U-anomaly) identified by Eggen (1958). The Hercules stream is an excess of stars with negative U velocities (away from the Galactic center, GC) that also move slower than the Sun's velocity by $V \sim -50\,\mathrm{km\,s^{-1}}$. Dehnen (1998) used main-sequence stars from *Hipparcos* and separated them in $B-V$, showing that Hercules is prominent at $B-V > 0.6$. Therefore, this stream is likely to have a dynamical origin both due to the stars being older than $\sim$ 4 Gyr (Antoja et al. 2008) and because they have a wide range of metallicities (Raboud et al. 1998; Bensby et al. 2007).

A mechanism to explain the dynamical origin of the Hercules stream was proposed by Dehnen (2000), who suggested that these stars reach the SNd on orbits due to the Outer Lindblad resonance (OLR) of the Galactic bar. In this scenario, the OLR needs to be placed close to the Sun, implying a pattern speed of the bar of ~1.85 times the local circular frequency (Antoja et al. 2014; Monari et al. 2017b).

This model for the Hercules stream fits well with a short and fast-rotating bar, whose extension is between 3.0 and 3.5 kpc (Binney et al. 1997; Bissantz & Gerhard 2002) with a pattern speed in the range of $50-65\,\mathrm{km\,s^{-1}\,kpc^{-1}}$ (Englmaier & Gerhard 1999; Fux 1999). However, recent measurements show that the Galactic long bar extends to 5.0 ± 0.2 kpc from the Galactic center (Wegg et al. 2015), and from new dynamical modeling of the stellar kinematics of the inner Galaxy, the pattern speed is $39\pm3.5\,\mathrm{km\,s^{-1}\,kpc^{-1}}$ (Portail et al. 2017). Then, the OLR is placed at $\sim$ 10.5 kpc, too far outside the SNd for the Hercules stream to be explained by OLR orbits.

In this Letter, we revisit the origin of the Hercules stream and show that these stars in the SNd can be naturally explained in the framework of such a slow bar. In this interpretation, the Hercules stream is made of stars orbiting the Lagrange points of the Galactic bar that reach the SNd while moving outward from the corotation (CR) region.

This work is organized as follows. In Section 2, we

describe our made-to-measure dynamical model of the Galaxy and the data we employed. In Section 3, we show that the Hercules stream naturally arises in this model, discuss which kind of orbits cause the secondary peak in the SNd velocity distribution, and how the prominence of the Hercules stream changes with Galactocentric distance and metallicity. We summarize and discuss our results in Section 4.

2. MODEL AND DATA

2.1. *Dynamical model of the Galaxy*

Recently, Portail et al. (2017) presented the first non-parametric dynamical model of the entire bar region. Using the Made-to-Measure (M2M) method (De Lorenzi et al. 2007; Portail et al. 2015), they adapted the particle weights of a self-consistent N-body model of the Galaxy in order to match data from numerous surveys. Their model successfully reproduces the 3D density of RCGs in the bulge from Wegg & Gerhard (2013); the magnitude distributions of RCGs across the bar region from the combination of the VVV, UKIDSS, and 2MASS surveys (Wegg et al. 2015); stellar kinematics from the BRAVA (Kunder et al. 2012), OGLE-II (Sumi et al. 2004), and ARGOS (Freeman et al. 2013; Ness et al. 2013) surveys; and the outer rotation curve up to 10 kpc (Sofue et al. 2009).

A few adjustments to the fitted and phase-mixed model of Portail et al. (2017) are required in order to study the influence of the galactic bar on the SNd. First, we increase the resolution of the model by a factor of 10, using a variant of the resampling algorithm presented in Dehnen (2009) because originally only $\sim$ 650 particles lay within 600 pc from the Sun. Second, the radial dispersion of the outer disk unconstrained in Portail et al. (2017) and is found after M2M fitting to be $\sigma_U = 44\,\mathrm{km\,s^{-1}}$, larger than the observed $\sim 36\,\mathrm{km\,s^{-1}}$ (see Section 2.2). Large radial dispersion in the disk is the result of orbits with large epicycle motions around their guiding centers. We thus cool the outer disk by evolving it for $\sim$1 Gyr, during which we apply a damping term in the radial equation of motion for particles with guiding radius > 6.5 kpc. The additional radial drag force used is $\dot{\mathrm{v}}_R = -2\,\lambda\,\mathrm{v}_R$, where $\lambda = 2.5\,\mathrm{Gyr^{-1}}$ is the timescale of the disk cooling, and v_R the radial velocity of the particle. Once the disk is cooled, we reproduce the M2M fitting of Portail et al. (2017), resulting in a nearly identical bar model, but with a high-resolution disk and a local radial dispersion of $35.5\,\mathrm{km\,s^{-1}}$, in good agreement with the data.

In this model, the Sun is located at a distance $R_0 = 8.2$ kpc (Bland-Hawthorn & Gerhard 2016) from the GC. The bar rotates at a pattern speed of $\Omega = 39\,\mathrm{km\,s^{-1}\,kpc^{-1}}$ and is oriented at an angle of $\alpha = 28°$ with the Sun–GC line of sight, consistent with the measurements of Wegg & Gerhard (2013) and Wegg et al. (2015) in the bulge and the long bar, respectively. The mass distribution of the model is such that the local circular velocity is $V(R_0) = 243\,\mathrm{km\,s^{-1}}$. Assuming a peculiar motion of the Sun with respect to the local circular orbit of $(U_0, V_0, W_0) = (11.1, 12.24, 7.25)\,\mathrm{km\,s^{-1}}$ (Schönrich et al. 2010), the total tangential velocity of the Sun is $255\,\mathrm{km\,s^{-1}}$ in approximate agreement with recent measurements (Reid & Brunthaler 2004; Bovy et al. 2012; Schönrich 2012; Reid et al. 2014). The face-on projection of the model is shown in Figure 1, together with the spatial coverage of the data described in the next subsection.

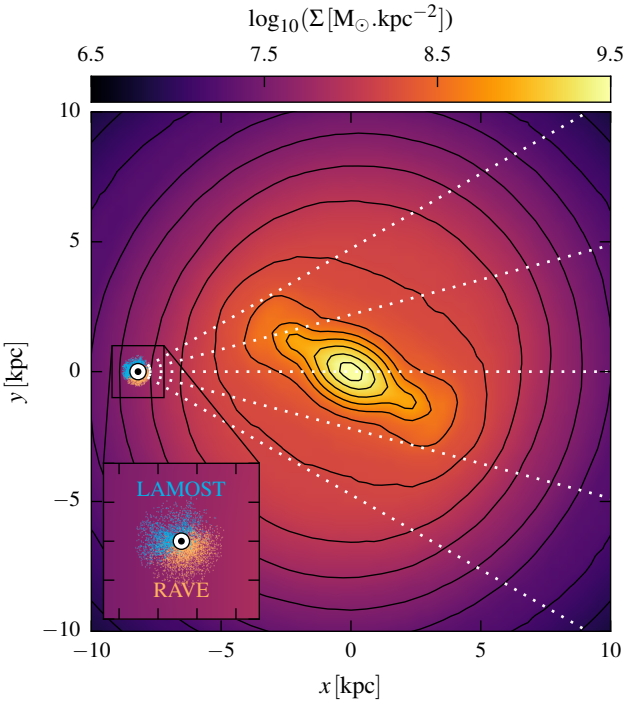

Figure 1. Face-on projection of the dynamical model of the galactic bar based on the work of Portail et al. (2017). Sightlines from the Sun (large dot) are indicated for Galactic longitudes of $l = -30°, -15°, 0°, +15°$, and $+30°$. The insert shows a zoom of the SNd where blue and yellow dots indicate the coverage of the TGAS+RAVE and TGAS+LAMOST data, respectively.

2.2. *6D phase-space data of SNd stars*

After one year of observation, the *Gaia* mission (Prusti et al. 2016) recently released its first set of data (Brown et al. 2016) including the Tycho-Gaia Astrometric Solution (TGAS; Michalik et al. 2015), a large catalog of accurate astrometry, parallaxes, and proper motions for more than 2×10^6 stars. Many of these TGAS stars have also been independently observed by spectroscopic surveys such as RAVE (DR5; Kunder et al. 2017) and LAM-

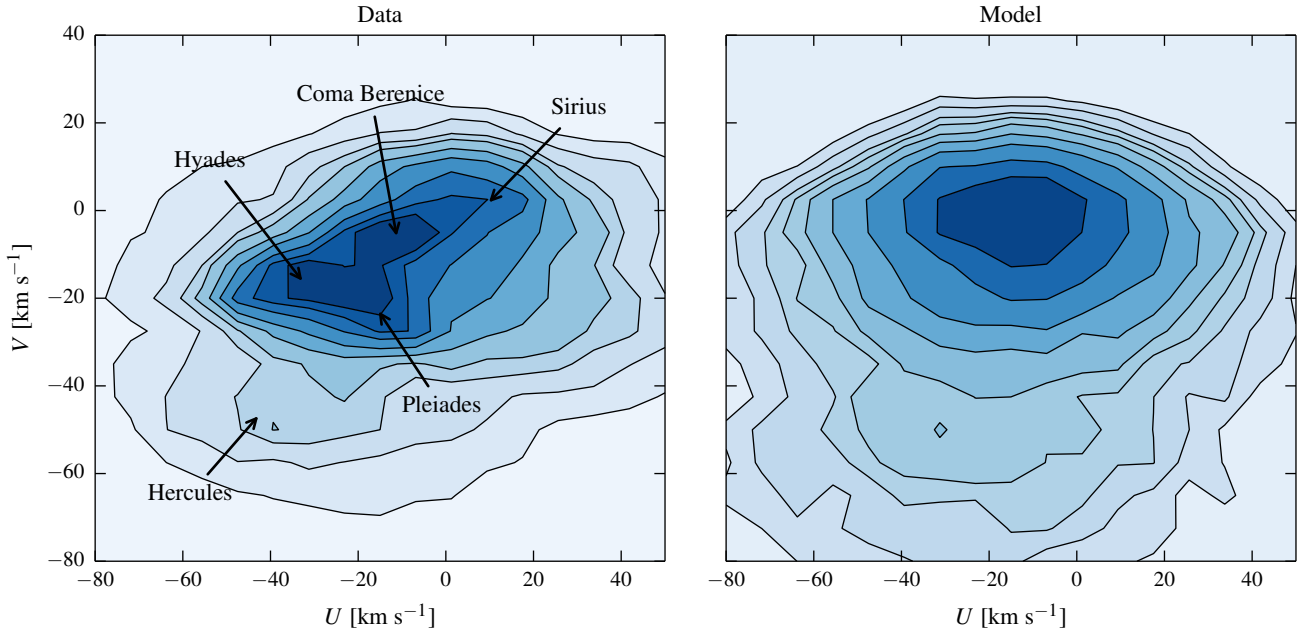

Figure 2. Velocity distribution in the SNd U–V-plane (relative to the Sun) for the data catalog (left) and the cross-matched model (right) within 300 pc from the Sun. The LSR is put at $U = -11.1\,\mathrm{km\,s^{-1}}$, $V = -12.24\,\mathrm{km\,s^{-1}}$. The contours contain, from inside outward, 10%, 20%, 30%, 40%, 50%, 60%, 80%, 90% of the stars (left) or model particles (right).

OST (star catalog from DR2; Liu et al. 2014), providing measurements for the radial velocities and metallicities of the stars.[1] Thus, by cross-matching TGAS with RAVE and/or LAMOST, we construct a catalog of 6D phase-space positions and metallicities of stars in the SNd. We limit ourselves to stars within 600 pc from the Sun with parallax errors smaller than 20%. For stars that have been observed spectroscopically multiple times (common stars between RAVE and LAMOST, or stars observed multiple times in RAVE), we use as the radial velocity and metallicity the weighted mean of the various measurements available. Our final catalog has 153,767 stars covering the SNd well, as displayed in Figure 1. Finally, the R.A., decl, parallax, proper motions on the sky, and radial velocity of the stars are converted to Cartesian Galactic phase-space positions and velocities using `galpy` python tools (Bovy 2015).

2.3. *Cross-Matching Model and Data*

Despite the increased resolution of the disk resulting from the resampling in Section 2.1, the number of particles is too low to represent the velocity distribution in the SNd with sufficiently low noise. Therefore, we created a catalog of 2×10^6 particles by integrating the model in its frozen potential and recording all particles within 600 pc from the Sun every 20 Myr, the average time for particles to cross the SNd. This produces a large, time-averaged catalog and requires an integration time of 2 Gyr given our resolution.

In order to approximate the selection function of the data, we construct a cross-matched catalog, selecting from the particle catalog the nearest particle in space to each star from the data catalog. If this results in a duplicate selection, the next unselected particle is used. Henceforth, we will employ our cross-matched catalog where the number of particles is equal to the number of stars in our data catalog.

3. HERCULES STREAM IN THE MODEL

In our model, the bar pattern speed is $39\,\mathrm{km\,s^{-1}\,kpc^{-1}}$, implying that the CR and OLR radius are at 6 kpc and 10.5 kpc, respectively. Can a model with this value of pattern speed cause a bimodal velocity distribution? Which kind of orbits could generate a bimodality in the U–V-plane? In this section, we answer these questions and consider how the Hercules stream changes with Galactic radius and metallicity.

3.1. *Comparison between Model and Data*

In Figure 2, we compare the SNd velocity distribution (U–V-plane) in the data (left) and in the model (right) within 300 pc from the Sun. We can see that the model naturally shows an excess of particles at $U \sim -30\,\mathrm{km\,s^{-1}}$, $V \sim -50\,\mathrm{km\,s^{-1}}$ in good agreement with Hercules. We note that the SNd velocity distribution has not been fitted but is a prediction.

[1] The LAMOST velocities are corrected by $5.7\,\mathrm{km\,s^{-1}}$ following Tian et al. (2015)

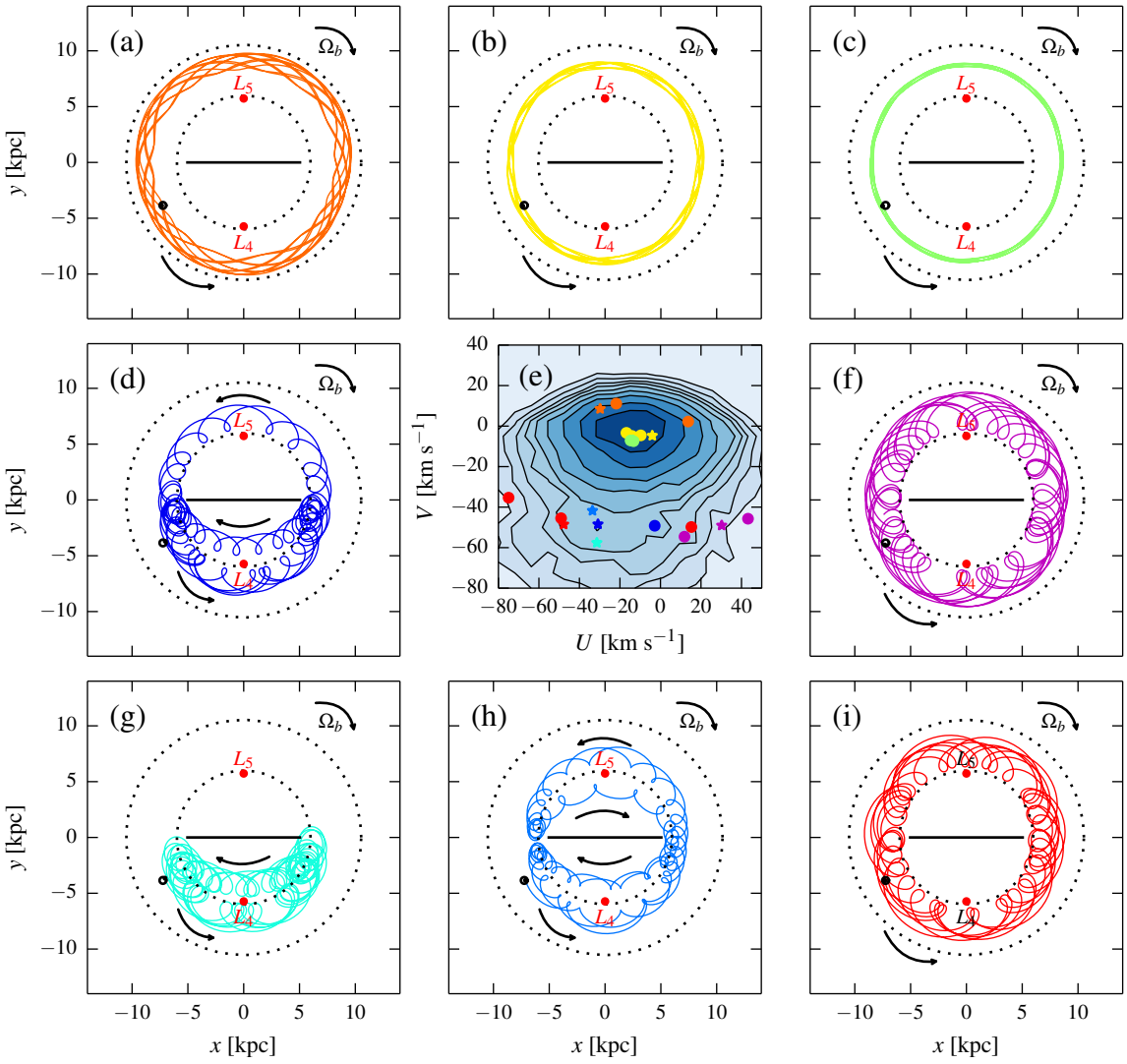

Figure 3. ((a)-(c)) Representative orbits in the frame corotating with the bar for the main component. ((d),(g),(h)): Hercules stream orbits in the frame corotating with the bar. (e) Velocity distribution of the model within 300 pc from the Sun. The initial U–V-position where a particle is selected to construct its orbit is marked as a star, and the dots with the same color show the U–V-positions where that particle again crosses the SNd during its orbit. Each color represents a different orbit. (d) An orbit near the Hercules density peak. (f) An orbit with opposite sign of U with respect to (d). (i) Similar to (d), but at $U \simeq -50\,\mathrm{km\,s^{-1}}$. The inner and outer dotted circles show the locations of the CR and OLR, respectively, and the red dots mark the positions of L_4 and L_5. The horizontal solid line shows the extension of the bar. The arrows along the orbits indicate the direction of motion in the corotating frame, while the arrows in the top right corner indicate the rotation of the bar in the inertial frame.

In the observed U–V-plot, we can clearly identify several maxima in the main velocity component, including the Sirius and Pleiades–Hyades moving groups. These moving groups have been linked to a dynamical origin (Famaey et al. 2008) induced by either the bar (Minchev et al. 2010), spiral arms (De Simone et al. 2004; Quillen & Minchev 2005; Antoja et al. 2011), or a mix of both (Chakrabarty 2007; Antoja et al. 2009).

The main component in the model does not contain these maxima; however, this may be because this model does not include spiral arms. The average V velocity of these model stars is also roughly $10\,\mathrm{km\,s^{-1}}$ larger than the circular velocity, due to streaming velocities induced in the bar. We estimated the radial velocity gradient in the model, $\frac{\partial <V_R>}{\partial R} = C + K \approx -3.2 \pm 0.8\ \mathrm{km\,s^{-1}\,kpc^{-1}}$, and the Oort constants $C \approx -2.9\ \pm 0.6\,\mathrm{km\,s^{-1}\,kpc^{-1}}$ and $K \approx -0.3\ \pm 0.6\,\mathrm{km\,s^{-1}\,kpc^{-1}}$, using local binned mean velocities and their gradients. $\frac{\partial <V_R>}{\partial R}$ is at the lower end of measurements from RAVE (Siebert et al. 2011) and smaller than in *Gaia* DR1, $C + K \approx -6.6\,\mathrm{km\,s^{-1}\,kpc^{-1}}$ (Bovy 2017).

To investigate further how these features and measure-

ments could be explained and fitted in a more elaborate model is outside the scope of this Letter. Here, we concentrate on showing that the Hercules stream is a consequence of the bar and on understanding the orbits that are at its origin.

3.2. *Which orbits cause the bimodality in the U–V-plane?*

We have integrated for 5 Gyr in the rotating frozen potential a subset of the model particles within 300 pc of the Sun. Figure 3 shows the U–V-distribution in the SNd (Figure 3(e)) from which we select orbits in the main component and in Hercules. The position in the U–V-plane where an orbit was started (at its coeval x, y position) is represented by a star. Orbits in the main component (Figure 3(a)-(c)) never cross the CR radius, and in general they have variable-sized epicycle motions around their guiding center. On the other hand, orbits in Hercules (Figure 3(d), (g), (h)) have energies allowing them to cross the CR radius. In this region a class of orbits appears around the Lagrange points L_4 and L_5 on the minor axis of the bar that can be stable (the Lagrange points aligned with the bar, L_1 and L_2, are unstable). Figure 3(d) shows an orbit selected near the peak Hercules density. Note that the orbit with opposite sign of U (Figure 3(f)) is radially extended but remains outside CR, as does the orbit in Figure 3(i). These orbits provide a constant background in the U–V-plot at negative V.

The Lagrange orbits librating around L_4 and L_5 have a banana-like shape parallel to the bar (Contopoulos & Grosbol 1989). In Hercules, we found mainly three kinds of Lagrange orbits: pure banana-like orbits orbiting around L_4, orbits that circulate L_4 and L_5, and orbits that move around CR for a while but then they get trapped by the L_4 or L_5 Lagrange point. The latter two classes are probably chaotic orbits. All three classes visit the SNd, but only rarely as their V-velocity in the corotating frame is small. They cross the SNd with $U < 0$ moving outward, in contrast to a perturbed axisymmetric distribution function just outside corotation in slow bars (Monari et al. 2017a), which has a symmetric feature in U with $V < 0$.

3.3. *Hercules at Different Galactic radii*

With the entire sample of stars that we have in our data catalog around the SNd within 600 pc from the Sun, we can make cuts in galactocentric distance in order to determine where the Hercules stream can be detected. We make three square bins of 400 pc, where the center of each bin, in Cartesian coordinates with respect to the GC, in kpc, is $(x, y) = (-8.6, 0), (-8.2, 0)$, and $(-7.8, 0)$. Because the Hercules stream is formed by stars that travel from the inner Galaxy to the SNd, we should expect it to be most prominent in the innermost bin.

In Figure 4, we show the velocity distribution in the three square bins for the data (top) and the model (bottom). In the data, Hercules is indeed most prominent in the inner bin, is still clearly present in the middle bin centered at the Sun's position, and then is almost absent in the outer bin only a few 100 pc outside the solar radius. The same trend is present in our model: Hercules is very clear in the innermost bin, and it disappears in the outermost bin. Therefore, our new interpretation is consistent with the observed variation of the strength of Hercules at different Galactocentric radii. Bovy (2010), Antoja et al. (2014) and Monari et al. (2017b) considered the position of the "gap" between the main component and Hercules as function of galactocentric distance. For all bins in Figure 4, we estimated the position of the gap as function of distance, by looking for a minimum or saddle point in the V-distribution, V_g (similar to Monari et al. 2017b). V_g decreases outward in both the data and the model, as indicated in Figure 4 but it is clear from the U–V-diagrams that further work is required to match quantitatively the Hercules peak inward from the Sun.

3.4. *The U–V-plane in Different metallicity ranges*

In our explanation, the stars in the Hercules stream come from around the bar's CR radius, implying that these stars should on average be older and more metal-rich than the SNd stars. This has indeed been observed by Liu (2016) for the LAMOST stars, even though as first shown by Raboud et al. (1998), the Hercules stars have a wide metallicity distribution.

In Figure 5, we show the U–V-velocity distribution for different metallicity intervals, $-0.5 <$[Fe/H]< -0.25 (top), $-0.25 <$[Fe/H]< 0.0 (middle), and $0.0 <$[Fe/H]< 0.25 (bottom) for the RAVE+TGAS sample. We did not use our entire catalog because the metallicity scale of the RAVE and LAMOST surveys is not the same. Figure 5 shows that Hercules is less conspicuous in the most metal-poor stars, but more prominent in the most metal-rich stars. Again this is consistent with the idea that the Hercules stars come from the inner Galaxy. A similar effect is seen in the main U–V-component where the Hyades and Pleiades groups dominate the most metal-rich stars, suggesting that also these stars mainly originate inside the solar radius.

4. SUMMARY AND DISCUSSION

The U–V-velocity distribution observed in the SNd is complex, and explaining every detail is not an easy task. This letter is devoted to giving a new explanation for the dynamical origin of the Hercules stream. The standard explanation for Hercules is that it is generated by orbits scattered by the OLR. However, this explanation requires the OLR to be close to the Sun (Dehnen 2000; Antoja et al. 2014; Monari et al. 2017b), which is incompatible

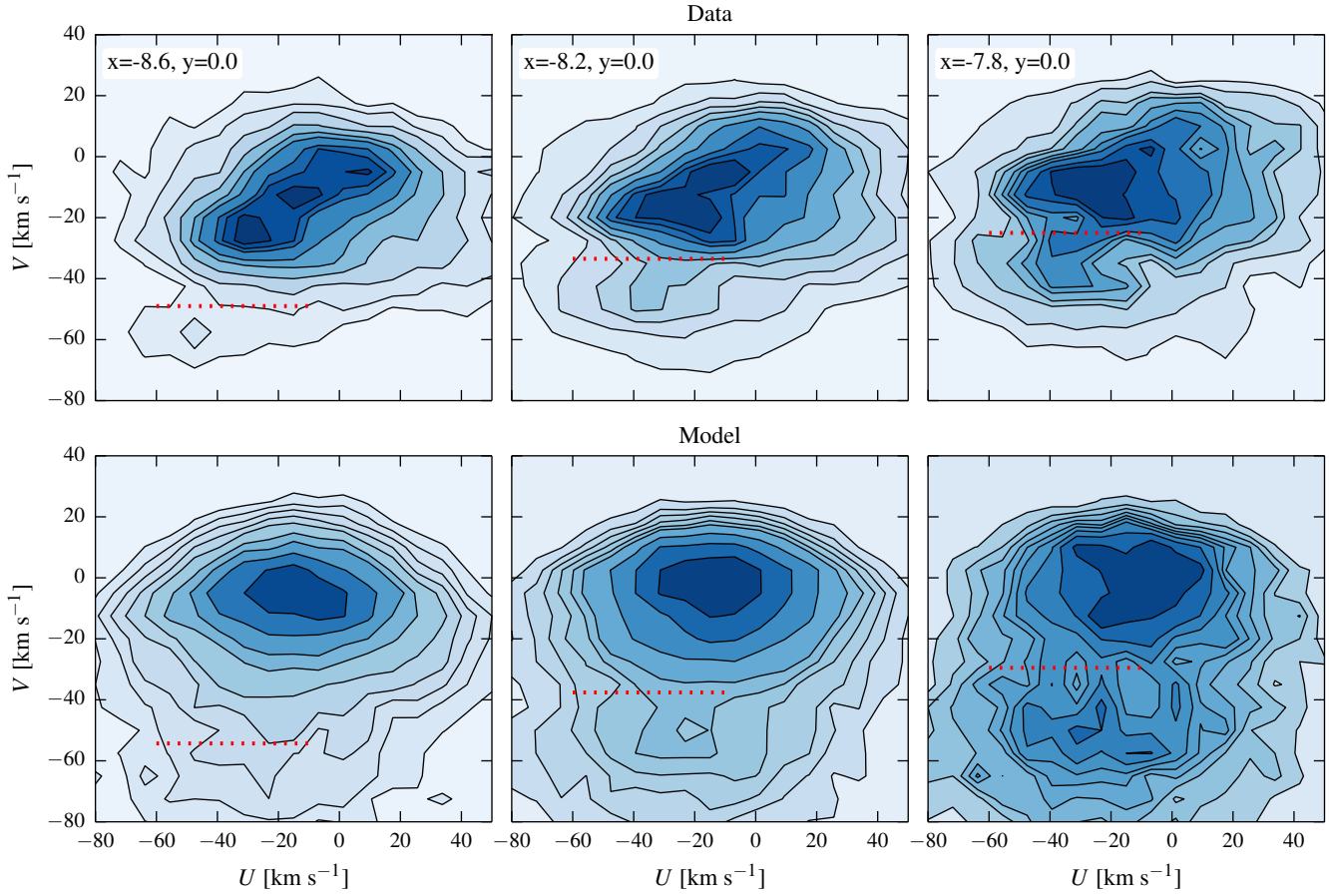

Figure 4. U–V-velocity distribution as function of Galactocentric distance, comparing data (top) and model (bottom). Each panel shows the velocity distribution in a square of 400 pc, moving inward toward the GC from left to right. The center of each square in Cartesian coordinates is indicated in the top left corner of the data panels. Horizontal red dotted lines indicate minima or saddle points in the V-distribution integrated over the range $U = [-60, -10]$ km s^{-1} where Hercules is most prominent. The contours are as in Figure 2.

with recent measurements of a lower pattern speed (Portail et al. 2017) and long bar (Wegg et al. 2015). For these low pattern speeds, the OLR is placed significantly beyond the SNd and cannot be responsible for the origin of Hercules.

We have analyzed the velocity distribution in the SNd using the best M2M particle model of the Galaxy of Portail et al. (2017) fitted to a variety of inner Galaxy data. This model has a bar pattern speed of 39 km s^{-1} kpc^{-1}. Without fitting the SNd velocity distribution, we find that this model naturally contains a secondary peak in the U–V-plane, which is consistent with the Hercules stream as seen in the TGAS-RAVE-LAMOST data. In the model, Hercules is mainly made of stars orbiting the Lagrange points near the bar's CR radius that have the right energies to visit the SNd. Some of these orbits circulate around L_4 only, but others go also to L_5.

Our new model naturally predicts that the Hercules stream is more prominent inward toward the GC and almost absent beyond a few 100 pc outward from the Sun, as seen in the TGAS-RAVE-LAMOST data. This trend may also be compatible with the OLR model (Bovy 2010; Antoja et al. 2014; Monari et al. 2017b). However, only the explanation advocated here is also consistent with the dynamics of the bar and bulge region. Our explanation also very plausibly describes the fact that the Hercules stars are more prominent in old and metal-rich stars, as seen in Liu (2016) and in Figure 5.

We do not yet understand how the substructure in the main distribution of SNd velocities arises in the context of the longer and slower bar and what role the Galactic spiral arms play in this. Better models of the SNd distribution function are also required to test whether the position in velocity of Hercules can change in space correctly. Understanding these points will be greatly aided by *Gaia* DR2, which will allow us to make U–V diagrams out to several kiloparsecs in the disk and provide definitive answers on the nature of Hercules and indeed all the dynamical streams in the disk.

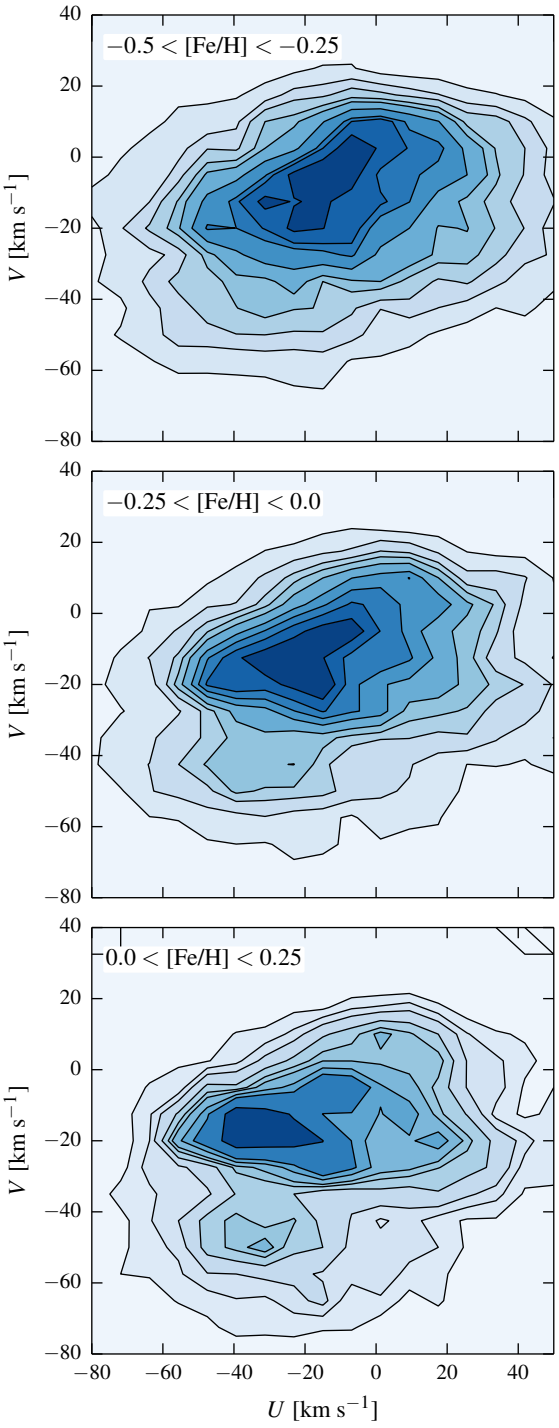

Figure 5. Velocity distribution of the TGAS + RAVE data in different metallicity intervals. The contours are as in Figure 2.

We thank Martin Smith for pointing out the paper by Tian et al. (2015) and Jo Bovy for making available his tool dealing with *Gaia* data. A.P.V. is grateful for a Conacyt postdoctoral fellowship and an MPE visiting fellowship. We also thank the anonymous referee for their careful reading and constructive comments. This work has made use of data from the European Space Agency *Gaia* mission (http://www.cosmos.esa.int/gaia), processed by the *Gaia* Data Processing and Analysis Consortium (DPAC), of RAVE data (www.rave-survey.org), and of data from the LAMOST survey of the Guoshoujing Telescope built by the Chinese Academy of Sciences (www.lamost.org).

REFERENCES

Antoja, T., Figueras, F., Fernández, D., & Torra, J. 2008, A&A, 490, 135
Antoja, T., Figueras, F., Romero-Gómez, M., et al. 2011, MNRAS, 418, 1423
Antoja, T., Valenzuela, O., Pichardo, B., et al. 2009, ApJL, 700, L78
Antoja, T., Helmi, A., Dehnen, W., et al. 2014, A&A, 563, A60
Bensby, T., Oey, M. S., Feltzing, S., & Gustafsson, B. 2007, ApJL, 655, L89
Binney, J., Gerhard, O., & Spergel, D. 1997, MNRAS, 288, 365
Bissantz, N., & Gerhard, O. 2002, MNRAS, 330, 591
Bland-Hawthorn, J., & Gerhard, O. 2016, ARA&A, 54, 529
Bovy, J. 2010, ApJ, 725, 1676
—. 2015, ApJS, 216, 29
—. 2017, MNRAS, 468, L63
Bovy, J., Allende Prieto, C., Beers, T. C., et al. 2012, ApJ, 759, 131
Brown, A. G. A., Vallenari, A., Prusti, T., et al. 2016, A&A, 595, A2
Chakrabarty, D. 2007, A&A, 467, 145
Contopoulos, G., & Grosbol, P. 1989, A&ARv, 1, 261
De Lorenzi, F., Debattista, V. P., Gerhard, O., & Sambhus, N. 2007, MNRAS, 376, 71
De Simone, R. S., Wu, X., & Tremaine, S. 2004, MNRAS, 350, 627
Dehnen, W. 1998, AJ, 115, 2384
—. 2000, AJ, 119, 800
—. 2009, MNRAS, 395, 1079
Eggen, O. J. 1958, MNRAS, 118, 154
—. 1996, AJ, 112, 1595
Englmaier, P., & Gerhard, O. 1999, MNRAS, 304, 512
Famaey, B., Siebert, A., & Jorissen, A. 2008, A&A, 483, 453
Freeman, K., Ness, M., Wylie-de Boer, E., et al. 2013, MNRAS, 428, 3660
Fux, R. 1999, A&A, 345, 787
Kunder, A., Koch, A., Michael Rich, R., et al. 2012, AJ, 143, 57
Kunder, A., Kordopatis, G., Steinmetz, M., et al. 2017, AJ, 153, 75
Liu, C. 2016, in Conf. Galact. Archaeol. Stellar Physics. Available https//www.aao.gov.au/conference/gasp16
Liu, X.-W., Yuan, H.-B., Huo, Z.-Y., et al. 2014, in Proc. IAU Symp. 298 Setting Scene Gaia LAMOST ed. S. Feltzing al. (Cambridge Cambridge Univ. Press. No. S298, 310–321
Michalik, D., Lindegren, L., & Hobbs, D. 2015, A&A, 574, A115
Minchev, I., Boily, C., Siebert, A., & Bienayme, O. 2010, MNRAS, 407, 2122
Monari, G., Famaey, B., Siebert, A., et al. 2017a, MNRAS, 465, 1443
Monari, G., Kawata, D., Hunt, J. A. S., & Famaey, B. 2017b, MNRAS, 466, L113
Ness, M., Freeman, K., Athanassoula, E., et al. 2013, MNRAS, 432, 2092
Portail, M., Gerhard, O., Wegg, C., & Ness, M. 2017, MNRAS, 465, 1621

Portail, M., Wegg, C., Gerhard, O., & Martinez-Valpuesta, I. 2015, MNRAS, 448, 713
Prusti, T., de Bruijne, J. H. J., Brown, A. G. A., et al. 2016, A&A, 595, A1
Quillen, a. C., & Minchev, I. 2005, AJ, 130, 576
Raboud, D., Grenon, M., Martinet, L., Fux, R., & Udry, S. 1998, A&A, 335, L61
Reid, M. J., & Brunthaler, A. 2004, ApJ, 616, 872
Reid, M. J., Menten, K. M., Brunthaler, A., et al. 2014, ApJ, 783, 130
Schönrich, R. 2012, MNRAS, 427, 274
Schönrich, R., Binney, J., & Dehnen, W. 2010, MNRAS, 403, 1829
Siebert, A., Famaey, B., Minchev, I., et al. 2011, MNRAS, 412, 2026
Sofue, Y., Honma, M., & Omodaka, T. 2009, PASJ, 61, 227
Sumi, T., Wu, X., Udalski, A., et al. 2004, MNRAS, 348, 1439
Tian, H.-J., Liu, C., Carlin, J. L., et al. 2015, ApJ, 809, 145
Wegg, C., & Gerhard, O. 2013, MNRAS, 435, 1874
Wegg, C., Gerhard, O., & Portail, M. 2015, MNRAS, 450, 4050